Visnyk NTUU KPI Seriia – Radiotekhnika Radioaparatobuduvannia, 2026, Iss. 104, pp. 15–22

UDC 621.376

Wideband Digital Frequency Synthesisers With Low Phase Noise Based on Single-Flux Quantum Logic Elements

Novak O. M., Kychak V. M.

Vinnytsia National Technical University, Vinnytsia, Ukraine

E-mail: *noyak.oleksii@gmail.com*

The article studies the current state and prospects for the development of broadband digital frequency synthesisers with low phase noise based on superconducting logic elements and arrays of Josephson junctions. It is shown that current developments are progressing along three complementary lines: large-amplitude metrological JAWS systems, microwave and VHF RF-JAWS with integrated cryogenic filters, and digital RSFQ/xSFQ/xeSFQ spectrum shaping systems. The main unresolved problems are highlighted: parasitic leakage of the control signal to the output, dispersion and non-uniform excitation of long arrays, the complexity of scaling the digital front-end, and the lack of built-in self-calibration of the quantum capture mode. A hybrid DDSJAWS architecture is proposed, combining a multiphase or clock-free SFQ front-end, a segmented JAWS output array, a differential mirror compensation path, and an embedded low-frequency QLR self-calibration. Mathematical models are presented for estimating the residual phase shift in the segmented array, the noise transfer function of a band-pass delta-sigma modulator, and the reduction of the quantum capture operating area.

Keywords: Josephson effect; JAWS; RF-JAWS; RSFQ; xSFQ; digital frequency synthesis; phase noise; quantum trapping; cryogenic equalisation; single-flux quantum logic

DOI: 10.64915/RADAP.2026.104.15-22

Introduction

The synthesis of ultrahigh-frequency signals, millimetre and sub-terahertz bands with low phase noise is one of the key challenges in modern radio engineering. For radio astronomy systems, high-precision spectroscopy, 5G/6G transceivers, satellite communications and quantum measurement systems, sources that simultaneously provide a wide tuning range, high spectral purity, good amplitude linearity and reproducibility of parameters in time are required. On a traditional CMOS/SiGe platform, achieving such a combination of characteristics is complicated by the rapid increase in phase noise, jitter and requirements for multi-stage frequency multiplication. A physical alternative is the use of the non-stationary Josephson effect and SFQ-class logic elements, in which the frequency and pulse width are tied to fundamental constants [1–7].

The aim of the article is to build a complete synthesizer architecture suitable for broadband radiotechnical implementation. Therefore, based on an analysis of global developments, this article will identify what physical and circuit limitations currently hinder the development of superconducting frequency synthesizers, and will propose a new architecture that combines the quantum precision of JAWS with the digital flexibility of the SFQ front-end and provides phase noise reduction.

1 The Analysis of Research and Publications in Which the Solution of the Problem Was Initiated

1.1 Fundamental Prerequisites and Early Metrological Implementations

The fundamental basis of this direction is directly linked to B. Josephson work, in which new tunnelling effects in superconductors were predicted [31]. The practical application of this effect began to develop actively with the advent of a pulse-controlled programmable Josephson voltage standard [14]. The next step involved work on generating both DC and AC voltages on the JAWS platform [17], the development of isolated circuits for waveform synthesis [29], as well as the analysis of the technological principles of creating next-generation Josephson standards [11].

A separate branch was the application of Josephson sources in noise thermometry and related precision measurements [22], whilst a review of the state of Josephson metrology was performed in a review paper [7].

These publications laid down two principles that remain crucial to this day: first, the output voltage of a Josephson system can be quantum-defined; second, the amplitude accuracy is achieved not by the final calibration of the analogue DAC, but by the physics of the transitions themselves. It was precisely this conclusion that later made possible the transition from metrological standards to quantum-precise synthesizers for radio technical applications.

1.2 The Evolution of JAWS from Low-Frequency Standards to RF Synthesizers

The further development of JAWS-systems proceeded in two directions: increasing the output amplitude and extending the bandwidth. For precision measurements, works with 300-mV JAWS and research into precision measurements on such systems [8], analysis of operating reserves and control modes of pulsed JAWS [9], as well as experiments in a cryocooler without liquid helium [10] became important. A significant step forward was the use of multi-level pulse excitation, which improved the control of quantised pulses [1]. In parallel, works focused on radio-frequency applications appeared: quantum-precise synthesizers of radio-frequency signals for communication tasks [12], models of quantised pulse propagation in junction arrays [13], as well as an experimental demonstration of signal synthesis at the 1 GHz level [2]. Modelling and characterisation of superconducting circuits at 4 K [15] became an important engineering component.

The work [16] demonstrated a qualitative breakthrough in RF-JAWS capabilities: an open-circuit RMS voltage of 17.56 mV at a frequency of 1.005 GHz, using zero-forcing equalisation, which substantially reduced distortion of the current pulses. In [20] this approach was further developed through the use of integrated fifth-order superconducting diplexers, which increased the open-circuit RMS voltage at 1.005 GHz to 22 mV, while the amplitude gain relative to the previous state of the art was about 25%. Furthermore, in work [18] the role of cryogenic broadband diplexers as a separate functional unit is demonstrated, whilst in [24] the synthesis of quantum-precise modulated microwave signals is considered. In [26] JAWS technology was extended to the VHF range: 50 mV RMS was achieved at frequencies up to 50.05 MHz, and the error in the low-frequency region was investigated in detail. A general overview of the current state of Josephson-effect applications is presented in [28].

1.3 Optical and Cryogenic Data Input into Junction Arrays

A separate line of research is associated with moving the pattern generator closer to the superconducting zone or completely replacing electrical data input with optical input. The work [3] demonstrated the possibility of driving a Josephson junction array from a photodiode, while in [19] demonstrated an optically controlled JAWS with bipolar waveform synthesis. Subsequently, a linear pulse shaper with sub-gigahertz resolution for controlling superconducting circuits [6] showed that an optical platform can provide high-speed pulse-pattern generation with very low phase instability.

Cryogenic electrical data input is actively developing towards deeper integration with the JAWS array. In work [30] electrical excitation of a junction array from a cryogenic BiCMOS pulse-pattern generator at a rate of 30 Gbit/s was demonstrated for the first time, paving the way for a fully integrated JAWS. An additional confirmation of the scaling trend is the 300-mV JAWS chip proposed in [4], in which a Wilkinson power divider and conical structures are used to achieve a more uniform distribution of microwave excitation.

1.4 Digital Superconducting Logic, Modelling, and Supporting Infrastructure

In parallel with JAWS developments, superconducting digital logic has also evolved. For quantum computer control systems, the SFQ controller DigiQ was proposed [21], proving the suitability of superconducting logic for complex digital coordination of a large number of signals. For the circuit analysis of Josephson circuits as distributed flow systems, the generalised flow-based circuit theory [23] is of great importance. From the CAD support perspective, a significant step forward was the introduction of models that explicitly account for the flow quantisation condition in the Keysight ADS environment [25], bringing standard EDA tools closer to the practical needs of superconducting circuit design.

An important problem in RSFQ-systems remains route balancing and the associated excess number of DFF elements. In work [27] it is shown that multi-phase clocking allows a significant reduction in the number of DFFs and the number of Josephson junctions; under the seven-phase approach, the average reduction in the number of junctions relative to the two-phase architecture was approximately 59.94%. Thus, the digital SFQ front-end is gradually acquiring the properties required for integration with JAWS as the output quantum DAC.

2 Identification of Unsolved Aspects of the General Problem

Despite significant progress, the problem of wideband frequency synthesis with low phase noise based on superconducting logic elements has not yet been fully resolved. Firstly, most modern JAWS systems are oriented toward metrology and use a complex external pulse-shaping path, whereas SFQ and RSFQ controllers rarely achieve the output quantum-precise voltage generation [12, 16, 20, 21].

Secondly, parasitic feedthrough of the control signal to the output port remains a key practical problem. Although digital and analogue equalisation, as well as integrated diplexers, significantly reduce this effect, they do not eliminate the mechanism of coherent addition of the parasitic component to the useful quantum voltage [16, 20, 26].

Thirdly, when scaling junction arrays, dispersion, mismatches, internal reflections, and excitation nonuniformity along the waveguide increase. This directly narrows the quantum trapping ranges and complicates the stable formation of a wideband spectrum [2, 13, 15, 29].

Fourthly, modern systems lack a closed-loop self-calibration circuit that would use low-frequency information about QLR to automatically adjust FIR equalizers, amplitude-phase balance, and the array operating point in real time [16, 20, 26].

3 Research Material

3.1 Basic Physical Model of Quantum Synthesis

The operation of a superconducting frequency synthesiser is based on the non-stationary Josephson effect, according to which the oscillation frequency in the junction is strictly determined by the applied voltage

$$f_J = K_J U = \frac{2e}{h} U. \tag{1}$$

Unlike classical self-excited oscillators, in which the resonator quality factor, the nonlinearity of the active element, and temperature drift play a central role, in the Josephson approach the frequency is related to fundamental constants. For the junction described by the RCSJ model, the current can be written as

$$I(t) = I_c \sin\varphi + \frac{\Phi_0}{2\pi R}\frac{d\varphi}{dt} + C\frac{\Phi_0}{2\pi}\frac{d^2\varphi}{dt^2}, \tag{2}$$

where I_c is the critical current, R is the normal resistance, C is the intrinsic capacitance of the junction, and φ is the phase difference. Each control pulse, provided that the array operates in the quantum trapping mode, generates an SFQ pulse with an area of

$$\int V(t)dt = \Phi_0 = \frac{h}{2e}. \tag{3}$$

For an array of N series-connected junctions, the average voltage in the pulse control mode is defined as

$$V_{avg} = \pm N f_{clk} \Phi_0 D, \tag{4}$$

where f_{clk} is the clock frequency of the pulse driver, D is the effective density of positive or negative pulses in the pattern.

In real RF-JAWS, the output voltage is the convolution of the discrete pattern with the impulse response of the array [13, 16, 20, 26]. It is this formula that indicates a linear increase in the useful voltage with an increase in the number of junctions and the clock frequency, but at the same time explains why long arrays are extremely sensitive to dispersion, reflections, and excitation inhomogeneity non-uniformity [2, 4, 15].

3.2 Concept of Hybrid DDS-JAWS Architecture

The proposed four-level hybrid DDS-JAWS synthesiser architecture is shown in Figure 1.

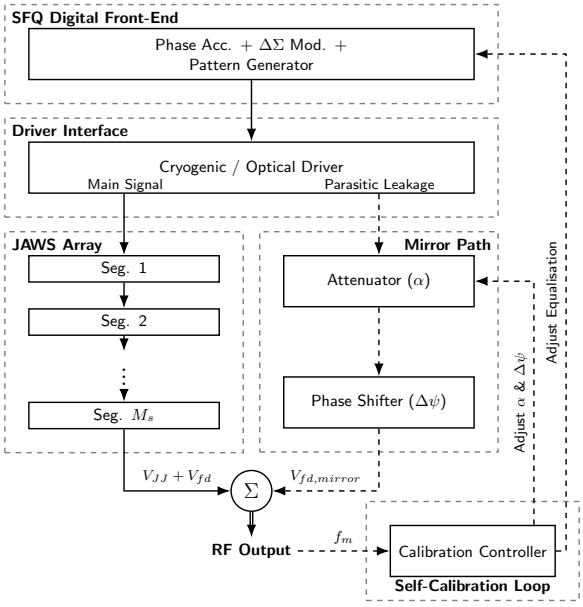

Fig. 1. Structural scheme of the proposed hybrid DDS-JAWS architecture

The first level is a digital superconducting front-end based on xSFQ/xeSFQ or multiphase RSFQ. Its purpose is to generate the frequency code, accumulate the phase, implement ΔΣ-modulation, perform pulse shaping and distribute pulse patterns among the array segments. For digital direct synthesis at this level, the standard relation is used

$$f_{out} = \frac{M}{2^N} f_{clk}, \tag{5}$$

where M is the tuning word, N is the bit width of the phase accumulator.

The discrete phase update can be given as $\varphi[n+1] = (\varphi[n] + M) \pmod{2^N}$. Unlike the classical DDS, there is no conventional DAC after the phase accumulator. Instead, a pulse code for the quantum output array is generated. The use of a multiphase approach reduces excessive route balancing and the number of DFF elements in the front-end [21, 27].

The second level is a cryogenic or optical driver that delivers the generated pattern to the JAWS array with minimal distortion, using BiCMOS serializers [30], or optical inputs [3, 6, 19].

The third level is a segmented JAWS array integrated into a coplanar waveguide. Segmentation allows a long-distributed structure to be divided into M_s locally matched sections. Each section contains N_s junctions, therefore the total number of transitions is $N = M_s N_s$. In each segment, local correction of the phase delay and pulse amplitude is provided, which can be implemented through controlled SQUID-elements or adjustable low-inductance superconducting lines.

The fourth level is a differential mirror compensation path. Unlike conventional equalisation, a corresponding channel next to the main JAWS array is formed here, in which quantisation is either absent or suppressed, while the parasitic component, close to that arising in the main channel, is preserved. After balanced subtraction, this component is significantly attenuated. Such an approach has not been described in the reviewed publications as an integral synthesiser architecture, which provides grounds for considering it a new direction in the development of this topic.

3.3 Analytical Model of Parasitic Feedthrough and Its Compensation

Let us denote the useful quantum voltage at the array output as V_{JJ}, and the parasitic component as V_{fd}. In a conventional RF-JAWS, the output signal can be represented as

$$V_{out} = V_{JJ} + V_{fd}. \tag{6}$$

Let us introduce the relative amplitude of the parasitic component $\rho = |V_{fd}|/|V_{JJ}|$. For small ρ the equivalent maximum phase error is estimated by the ratio

$$\Delta\varphi_{max} \approx \rho, \tag{7}$$

where $\Delta\varphi_{max}$ is expressed in radians. If the feedthrough level is L_{fd} dBc relative to the useful tone, then $\rho = 10^{(L_{fd}/20)}$.

For the level of -33 dBc, typical for RF-JAWS with integrated diplexers [20], we obtain $\rho \approx 0.022$, that is $\Delta\varphi_{max} \approx 0.022$ rad or about 1.3°. This already noticeably degrades the spectral purity of the synthesiser and changes the morphology of the QLR [20, 26].

For the proposed mirror path, the output voltage has the form

$$V_\Sigma = V_{JJ} + V_{fd} - \alpha V_{fd} e^{j\Delta\psi} = \\ = V_{JJ} + V_{fd}(1 - \alpha e^{j\Delta\psi}), \tag{8}$$

where α is the amplitude matching coefficient between the main and mirror paths, and $\Delta\psi$ is the residual phase mismatch between them. In physical terms, α characterises how accurately the parasitic component in the mirror channel reproduces the amplitude of the feedthrough component in the main channel, whereas $\Delta\psi$ describes the phase error between these two parasitic contributions. Therefore, the efficiency of the proposed compensation method is determined mainly by the accuracy of amplitude and phase balancing of the two paths

$$\rho_{res} = \rho|1 - \alpha e^{j\Delta\psi}|. \tag{9}$$

Hence, the additional attenuation of the parasitic component is

$$G_{comp} = -20\log_{10}|1 - \alpha e^{j\Delta\psi}|. \tag{10}$$

For example, at $\alpha = 0.95$ and $\Delta\psi = 5°$ the additional attenuation is about 20 dB, while at $\alpha = 0.99$ and $\Delta\psi = 2°$ it exceeds 25 dB. In this case, the initial parasitic feedthrough of -33 dBc can be reduced to approximately -55 dBc, decreasing the equivalent phase error by almost an order of magnitude. Importantly, this scheme specifically deals with the coherent parasitic component, which is the most difficult to eliminate by DSP-equalisation alone [16, 20, 26].

3.4 Segmentation of the JAWS Array and Estimation of the Internal Phase Shift

Let us consider a waveguide array of length L with an effective phase velocity v_p. For the upper operating frequency f_{max} the total phase shift along the array is

$$\Theta = \frac{2\pi f_{max} L}{v_p}. \tag{11}$$

If the array is divided into M_s segments, the phase shift within one segment will be defined as

$$\Theta_s = \frac{\Theta}{M_s} = \frac{2\pi f_{max} L}{v_p M_s}. \tag{12}$$

Figure 2 shows that segmentation rapidly changes from a technological option into a physical necessity as the upper synthesis frequency increases. In the 25–50 GHz range, the use of only one or two segments no longer provides sufficient excitation uniformity.

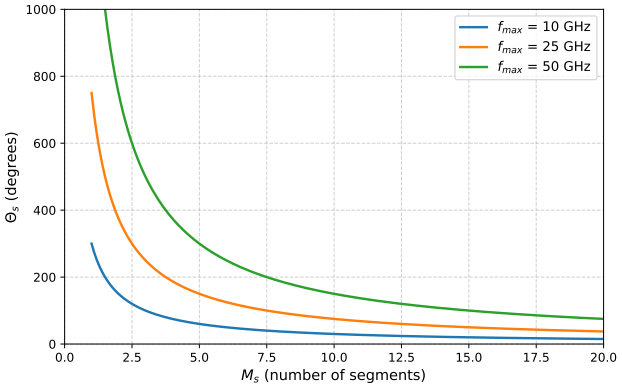

Fig. 2. Phase shift within one segment as a function of the number of segments M_s

To ensure relatively uniform excitation within a segment at the stage of preliminary design, it is reasonable to require $\Theta_s \leq \pi/5$. This condition should be considered as a first-order engineering estimate, since a complete description of a real JAWS array also depends on impedance matching, distributed capacitance and inductance, internal reflections, and technological non-uniformity of the junctions. Nevertheless, this simplified criterion is useful for estimating the minimum required number of segments and gives the following segmentation condition

$$M_s \geq \frac{10 f_{max} L}{v_p}. \tag{13}$$

For a chip length of $L = 1$ mm and an effective phase speed $v_p = 1.2 \cdot 10^8$ м/с for $f_{max} = 25$ GHz we obtain $M_s \geq 3$, and for $f_{max} = 50$ GHz – $M_s \geq 5$. For a chip length of $L = 10$ mm for $f_{max} = 25$ GHz we already need $M_s \geq 21$ elements, and for $f_{max} = 50$ GHz – $M_s \geq 42$ elements.

Thus, the required number of segments increases linearly with the active length of the JAWS-array and the upper operating frequency. For compact millimetre-scale structures, a few segments are sufficient, whereas centimetre-scale distributed arrays require a multi-segment architecture with dozens of locally matched sections. This imposes additional requirements on synchronisation, phase alignment, local equalisation, and QLR self-calibration.

The effective coefficient of coherent voltage summation within a segment can be estimated as

$$\eta_{seg} \approx \left| \frac{\sin(\Theta_s/2)}{\Theta_s/2} \right|. \tag{14}$$

For small Θ_s the coefficient η_{seg} tends to unity, whereas increasing Θ_s leads to a loss in the useful-tone amplitude and a narrowing of the operating QLR. Therefore, segmentation directly increases both the useful amplitude and the stability of spectral characteristics [2, 13].

3.5 Model of a Multi-Phase SFQ Front-End and the Condition for Reducing Hardware Complexity

For direct digital synthesis on an SFQ-platform, a significant problem is the excessive number of DFF elements required for path balancing. In the multi-phase approach, the load frequency per phase channel decreases approximately as

$$R_P \approx \frac{f_{clk}}{P}, \tag{15}$$

where P is the number of phases. However, the number of balancing elements decreases the total number of junctions in the digital front-end also decreases [27]. If $N_{JJ}^{(1)}$ denotes the number of junctions in the single-phase front-end, and $\beta(P)$ denotes the structural reduction coefficient, then

$$N_{JJ}^{(P)} = \beta(P) N_{JJ}^{(1)}, \quad 0 < \beta(P) < 1. \tag{16}$$

According to [27], the transition to a seven-phase circuit can provide $\beta \approx 0.40$ relative to a push-pull architecture, i.e. approximately 60% reduction in the number of junctions. For a frequency synthesiser, this means not only a more compact digital front-end, but also fewer sources of internal jitter and lower requirements for global clock distribution.

3.6 Delta-Sigma Modulation, Noise Transfer Function and Multilevel Pulse Shaping

For wideband signal synthesis, the JAWS system cannot be limited to a simple uniform pulse stream. It is necessary to generate a spectrally optimised pattern that pushes the quantisation noise outside the narrow operating band. In a simplified form, for a fourth-order band-pass $\Delta\Sigma$-modulator cantered at the frequency f_t the normalised noise transfer function can be written as

$$|NTF(f)| = \left| 1 - 2\cos\left(\frac{2\pi f_t}{f_{clk}}\right) z^{-1} + z^{-2} \right|^4, \quad z = e^{j2\pi f/f_{clk}}. \tag{17}$$

It is precisely this dependence that forms the basis of the graph in Fig. 3. It forms a spectral “notch” near the target frequency and ensures the transfer of a significant portion of the noise into adjacent bands [20, 26].

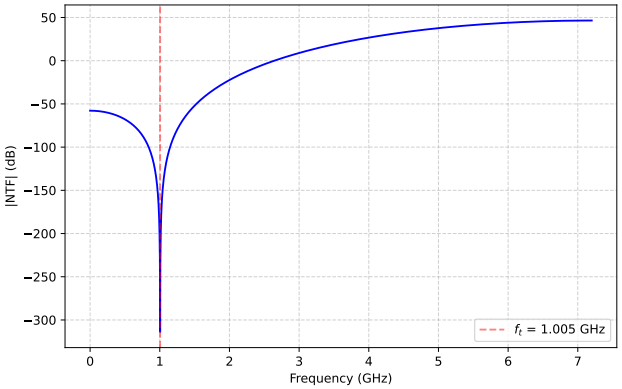

Fig. 3. Normalised noise transfer function of a fourth-order band-pass ΔΣ modulator

If the pulse excitation has only three levels $\{-1, 0, +1\}$, the possibilities for additional spectral shaping of the excitation sequence remain limited. Therefore, it is reasonable to consider a transition to a five-level representation $\{-1, -0.5, 0, +0.5, +1\}$, in which intermediate levels are used for finer control of the pulse spectrum. In this interpretation, the additional pre- and post-pulse components do not change the basic quantum nature of the JAWS output, but make it possible to reduce the low-frequency and parasitic spectral components of the driving signal. Such a representation can be regarded as an auxiliary pulse-shaping approach that complements the ΔΣ pattern generation and cryogenic equalisation. In a first approximation, the time form of such a pulse can be represented as

$$I_p(t) = I_0 \mathrm{sinc}\left(\frac{t}{\tau}\right) - 0.5 I_0 \mathrm{sinc}\left(\frac{t - T_{clk}}{\tau}\right) - \\ - 0.5 I_0 \mathrm{sinc}\left(\frac{t + T_{clk}}{\tau}\right). \quad (18)$$

From the standpoint of practical implementation, it is important to note that the real pulse-shaping path is described by a cascade of transfer functions of room electronics $H_{RT}(f)$, cryogenic filters $H_{cryo}(f)$ and interelement connections $H_{int}(f)$. Therefore, full equalisation should compensate for the product

$$H_\Sigma(f) = H_{RT}(f) H_{cryo}(f) H_{int}(f). \quad (19)$$

In modern RF-JAWS this is performed in stages: EQ1 compensates the DAC, EQ2 compensates S-parameters of the cryogenic HPF diplexer, and EQ3 compensates residual cable and parasitic distortions [20]. In the proposed architecture, a fourth level is added to these three levels – a balanced compensation level, that addresses not the pulse shape itself, but the vector parasitic component.

3.7 Extended Quantum Trapping Model and Self-Calibration

In the vast majority of existing works, the QLR is analysed as a two-dimensional area in the I_{dc} – A_p coordinates, where A_p is the amplitude of the pulse excitation. For a wideband synthesiser, this representation is insufficient, since mode stability is also affected by parasitic feedthrough, path mismatches, temperature drift, and internal dispersion. It is therefore reasonable to introduce a generalised phenomenological model

$$\left(\frac{I_{dc} - I_0}{\Delta I}\right)^2 + \left(\frac{A_p - A_0}{\Delta A}\right)^2 + \left(\frac{\varepsilon}{\varepsilon_{cr}}\right)^2 \le 1, \quad (20)$$

where ε is a generalised structural error parameter, that includes residual path, mismatches, and temperature-time drift. For a fixed ε the cross-section of this area in the $I_{dc} - A_p$ plane has an elliptical shape with a normalised area

$$\frac{S(\varepsilon)}{S_0} = 1 - \left(\frac{\varepsilon}{\varepsilon_{cr}}\right)^2. \quad (21)$$

This dependence is used in Fig. 4. It shows that any reduction in ε due to better equalisation, segmentation, or differential compensation directly expands the operating quantum trapping area.

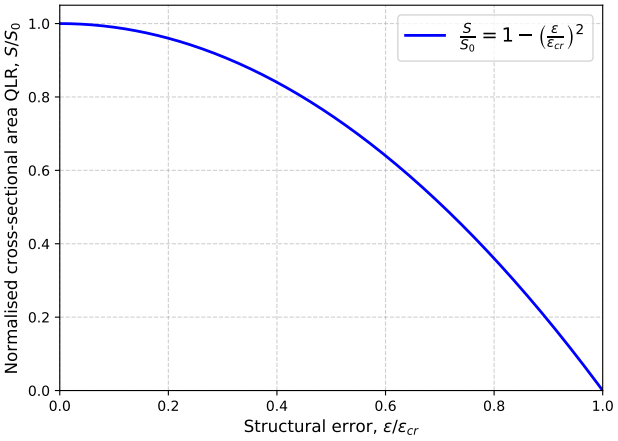

Fig. 4. Normalised cross-sectional area of the QLR as a function of the structural error ε_{cr}

Therefore, the issue of parasitic feedthrough should be considered not as a local spectrum improvement, but as a mechanism for increasing the operating margin of the entire synthesiser.

To automate this process, low-frequency QLR self-calibration is proposed. Its essence lies in the simultaneous synthesis of an operating high-frequency tone and an auxiliary control tone f_m in the low-frequency area. If P_m is the power of the auxiliary tone, and P_0 is its reference value at the centre of the QLR, then the quality criterion can be defined as

$$J = \left|\frac{P_m - P_0}{P_0}\right| + \lambda \left|\frac{V_{fd,res}}{V_J J}\right|, \quad (22)$$

where λ is the weighting coefficient that sets the trade-off between the QLR width and residual parasitic feedthrough. Minimisation of J can be performed by an

adaptive algorithm that adjusts EQ3, the mirror path balance, and the bias current I_{dc}. Unlike the manual procedure typical of modern systems [16, 20, 26], this approach makes the synthesiser more autonomous and suitable for field or industrial applications.

Conclusions

The article demonstrates that the current state of research of wideband frequency synthesisers based on superconducting logic elements is characterised by the convergence of three previously relatively independent directions: metrological JAWS-systems, microwave RF/VHF-JAWS, and digital SFQ/RSFQ/xSFQ-platforms. The main potential for further phase-noise reduction lies precisely at the intersection of these directions.

The main unresolved problems at present are:

- parasitic feedthrough of the control signal to the output and the associated vector phase error;
- dispersion degradation and non-uniform excitation of long junction arrays;
- excessive structural complexity of the traditional SFQ front-end;
- the absence of built-in QLR self-calibration.

These problems cannot be fully eliminated only by local equalisation or traditional filtering alone.

The main result of this work is the proposed concept of a hybrid DDS-JAWS architecture, which includes a multiphase SFQ front-end, a segmented JAWS array, a differential mirror path for parasitic feedthrough compensation, and a built-in low-frequency QLR self-calibration circuit. Based on the analytical study, it has been shown that additional architectural compensation of parasitic feedthrough by 20–25 dB can reduce the equivalent phase error by approximately an order of magnitude, while array segmentation directly reduces the internal phase shift and increases the voltage coherent summing coefficient.

Prospects for further research aimed at confirming the presented calculation results include: the development of a complete circuit model of the mirror compensation path; the selection of an optimal method of JAWS array segmentation in the 10–100 GHz range; a comparison of cryogenic BiCMOS and optical pulse injection; the development of a closed-loop self-calibration algorithm based on the QLR criterion; and experimental verification of the proposed solutions using an extended synthesiser model.

References

[1] Brevik J. A., Flowers-Jacobs N. E., Fox A. E. et al. (2017). Josephson Arbitrary Waveform Synthesis With Multilevel Pulse Biasing. *IEEE Transactions on Applied Superconductivity*, Vol. 27, No. 3. Art. 1301707. DOI: 10.1109/TASC.2017.2662708.

[2] Donnelly C. A., Flowers-Jacobs N. E., Brevik J. A. et al. (2020). 1 GHz waveform synthesis with Josephson junction arrays. *IEEE Transactions on Applied Superconductivity*, Vol. 30, No. 3. Art. 1400111. DOI: 10.1109/TASC.2019.2932342.

[3] Nissilä J., Fordell T., Manninen A. J., Govenius J., Kemppinen A. (2021). Driving a low critical current Josephson junction array with a high-speed current pulse pattern generated by a photodiode. *Applied Physics Letters*, Vol. 119, No. 3. Art. 032601. DOI: 10.1063/5.0060804.

[4] Jia W., Song J., Zhong Y. et al. (2025). A 300 mV Josephson Arbitrary Waveform Synthesizer Chip at NIM. *Applied Sciences*, Vol. 15, No. 21. Art. 11811. DOI: 10.3390/app152111811.

[5] O. P. Yanenko, K. L. Shevchenko, and V. M. Kychak (2020). Methods and means of formation, processing and use of lowintensity electromagnetic signals, monogr. Vinnytsya, Ukraine: VNTU, 268 p.

[6] Lee D., Nakamura T., Metcalf A. J. et al. (2023). Sub-GHz resolution line-by-line pulse shaper for driving superconducting circuits. *APL Photonics*, Vol. 8, No. 8. Art. 086115. DOI: 10.1063/5.0157003.

[7] Benz S. P., Hamilton C. A. (2004). Application of the Josephson effect to voltage metrology. *Proceedings of the IEEE*, Vol. 92, No. 10. pp. 1617–1629. DOI: 10.1109/JPROC.2004.833671.

[8] Benz S. P., Dresselhaus P. D., Burroughs C. J., Bergren N. F. (2007). Precision Measurements Using a 300 mV Josephson Arbitrary Waveform Synthesizer. *IEEE Transactions on Applied Superconductivity*, Vol. 17, No. 2. pp. 864–869. DOI: 10.1109/TASC.2007.898138.

[9] Houtzager E., Benz S. P., van den Brom H. E. (2009). Operating Margins for a Pulse-Driven Josephson Arbitrary Waveform Synthesizer Using a Ternary Bit-Stream Generator. *IEEE Transactions on Instrumentation and Measurement*, Vol. 58, No. 4. pp. 775–780. DOI: 10.1109/TIM.2008.2008471.

[10] Sosso A., Durandetto P., Trinchera B., Kieler O., Behr R., Kohlmann J. (2017). Characterization of a Josephson array for pulse-driven voltage standard in a cryocooler. *Measurement*, Vol. 95. pp. 77–81. DOI: 10.1016/j.measurement.2016.09.039.

[11] Benz S. P., Dresselhaus P. D., Burroughs C. J. (2001). Nanotechnology for next-generation Josephson voltage standards. *IEEE Transactions on Instrumentation and Measurement*, Vol. 50, No. 6, pp. 1513–1518. DOI: 10.1109/19.982937.

[12] Hopkins P. F., Brevik J. A., Castellanos-Beltran M. C. et al. (2019). RF Waveform Synthesizers With Quantum-Based Voltage Accuracy for Communications Metrology. *IEEE Transactions on Applied Superconductivity*, Vol. 29, No. 5. DOI: 10.1109/TASC.2019.2898407.

[13] Donnelly C. A., Brevik J. A., Flowers-Jacobs N. E. et al. (2019). Quantized Pulse Propagation in Josephson Junction Arrays. *IEEE Transactions on Applied Superconductivity*, DOI: 10.1109/TASC.2019.2929481.

[14] Benz S. P., Hamilton C. A. (1996). A pulse-driven programmable Josephson voltage standard. *Applied Physics Letters*, Vol. 68, No. 22, pp. 3171–3173. DOI: 10.1063/1.115814.

[15] Boaventura A. S., Williams D. F., Chamberlin R. A. et al. (2020). Microwave Modeling and Characterization of Superconductive Circuits for Quantum Voltage Standard Applications at 4 K. *IEEE Transactions on Applied Superconductivity*, Vol. 30, No. 2. DOI: 10.1109/TASC.2019.2963403.

[16] Babenko A. A., Flowers-Jacobs N. E., Lasser G. et al. (2021). A Microwave Quantum-Defined Millivolt Source. *IEEE Transactions on Microwave Theory and Techniques*, Vol. 69, No. 12, pp. 5404–5416. DOI: 10.1109/TMTT.2021.3121425.

[17] Benz S. P., Burroughs C. J., Dresselhaus P. D., Christian L. A. (2001). AC and DC Voltages From a Josephson Arbitrary Waveform Synthesizer. *IEEE Transactions on Instrumentation and Measurement*, Vol. 50, No. 2, pp. 181–184.

[18] Babenko A. A., Lasser G., Flowers-Jacobs N. E. et al. (2022). Cryogenic Decade-Passband Superconducting Integrated Diplexer. *2022 IEEE/MTT-S International Microwave Symposium (IMS)*. DOI: 10.1109/IMS37962.2022.9865615.

[19] Brevik J. A., Lee D., Fox A. E. et al. (2022). Bipolar Waveform Synthesis With an Optically Driven Josephson Arbitrary Waveform Synthesizer. *IEEE Transactions on Applied Superconductivity*, Vol. 32, No. 9. Art. 1400408. DOI: 10.1109/TASC.2022.3167660.

[20] Babenko A. A., Flowers-Jacobs N. E., Lasser G. et al. (2022). RF Josephson Arbitrary Waveform Synthesizer With Integrated Superconducting Diplexers. *IEEE Transactions on Applied Superconductivity*, Vol. 32, No. 8. Art. 1500909. DOI: 10.1109/TASC.2022.3201188.

[21] Jokar M. R., Rines R., Pasandi G. et al. (2022). DigiQ: A Scalable Digital Controller for Quantum Computers Using SFQ Logic. *2022 IEEE International Symposium on High-Performance Computer Architecture (HPCA)*, pp. 400–414. DOI: 10.1109/HPCA53966.2022.00037.

[22] Benz S. P., Martinis J. M., Dresselhaus P. D., Nam S. W. (2003). An AC Josephson source for Johnson noise thermometry. *IEEE Transactions on Instrumentation and Measurement*, Vol. 52, No. 2, pp. 545–549. DOI: 10.1109/TIM.2003.811687.

[23] Wang Y. (2023). A general flux-Based Circuit Theory for Superconducting Josephson Junction Circuits. *arXiv*, arXiv:2308.01693. DOI: 10.48550/arXiv.2308.01693.

[24] Babenko A. A., Flowers-Jacobs N. E., Fox A. E. et al. (2023). Quantum-Based Modulated Microwave Wwaveforms. *IEEE Transactions on Microwave Theory and Techniques*, Vol. 72, Iss. 4, pp. 2047–2056. DOI: 10.1109/TMTT.2023.3297364.

[25] Naaman O., Hassan M. A., White T. et al. (2025). Modeling Flux-Quantizing Josephson Junction Circuits in Keysight ADS. *IEEE Transactions on Applied Superconductivity*, Vol. 35, Iss. 2, pp. 1-11. DOI: 10.1109/TASC.2025.3528927.

[26] Thomas J. N., Flowers-Jacobs N. E., Fox A. E. et al. (2024). VHF Josephson Arbitrary Waveform Synthesizer. *IEEE Transactions on Applied Superconductivity*, Vol. 34, no. 7. Art. 1500810. DOI: 10.1109/TASC.2024.3418332.

[27] Bairamkulov R., De Micheli G. (2024). Towards Multiphase Clocking in Single-Flux Quantum Systems. *arXiv*, arXiv:2403.05884. DOI: 10.48550/arXiv.2403.05884.

[28] Benz S. P., Biesecker J., Burroughs C. J. et al. (2024). AC metrology applications of the Josephson effect. *Applied Physics Letters*, Vol. 125, No. 5. Art. 050501. DOI: 10.1063/5.0219991.

[29] Benz S. P., Burroughs C. J., Dresselhaus P. D. (2001). AC Coupling Technique for Josephson Waveform Synthesis. *IEEE Transactions on Applied Superconductivity*, Vol. 11, No. 1, pp. 612–616.

[30] Kudabay Y., Kieler O., Starkloff M. et al. (2025). Electrical Drive of a Josephson Junction Array Using a Cryogenic BiCMOS Pulse Pattern Generator: Towards a Fully Integrated Josephson Arbitrary Waveform Synthesizer. *arXiv*, arXiv:2512.20367. DOI: 10.48550/arXiv.2512.20367.

[31] Josephson B. D. (1962). Possible new effects in superconductive tunnelling. *Physics Letters*, Vol. 1, No. 7, pp. 251–253. DOI: 10.1016/0031-9163(62)91369-0.

Широкосмугові цифрові синтезатори частот із низьким фазовим шумом на одноквантових логічних елементах

Новак О. М., Кичак В. М.

У статті досліджено сучасний стан і перспективи побудови широкосмугових цифрових синтезаторів частот із низьким фазовим шумом на основі надпровідникових логічних елементів і масивів джозефсонівських переходів. Показано, що сучасні розробки розвиваються за трьома взаємодоповнювальними напрямами: метрологічні JAWS-системи великої амплітуди, мікрохвильові та VHF RF-JAWS з інтегрованими кріогенними фільтрами, а також цифрові RSFQ/xSFQ/xeSFQ-системи формування спектра. Виділено головні невирішені проблеми: паразитне проходження керуючого сигналу на вихід, дисперсію та неоднорідність збудження довгих масивів, складність масштабування цифрового фронтенда та відсутність вбудованої самокалібровки режиму квантового захоплення. Запропоновано гібридну DDS-JAWS архітектуру, що поєднує багатофазний або clock-free SFQ-фронтенд, сегментований вихідний JAWS-масив, диференційний дзеркальний тракт компенсації і вбудовану низькочастотну QLR-самокалібровку. Наведено математичні моделі для оцінювання залишкового, фазового набігу в сегментованому масиві, передавальної функції шуму смугового дельта-сигма модулятора та зменшення робочої області квантового захоплення.

Ключові слова: ефект Джозефсона; JAWS; RF-JAWS; RSFQ; xSFQ; цифровий синтез частот; фазовий шум; квантове захоплення; кріогенна еквалізація; одноквантова логіка